An Ultra-Wideband Body Area Propagation Channel Model—From Statistics to Implementation

Andrew Fort, *Student Member, IEEE*, Claude Desset, *Member, IEEE*, Philippe De Doncker, Piet Wambacq, *Member, IEEE*, and Leo Van Biesen, *Member, IEEE*

***Abstract*—Body worn wireless sensors for monitoring health information is a promising new application. In developing these sensors, a communication channel model is essential. However, there are currently few measurements or models describing propagation around the body. To address this problem, we have measured electromagnetic waves near the torso and derived relevant statistics. We find that components diffracting around the body are well modeled using correlated log normal variables, and a Nakagami-m distribution can be used to incorporate the influence of arm motions. We have implement this model and evaluated it in terms of important communication metrics. This paper describes body area propagation statistics and proposes a suitable computer model implementation.**

***Index Terms*—Body area network (BAN), propagation channel, ultra-wideband (UWB).**

I. Introduction

USING wireless sensors around the body to monitor health information is a promising new application made possible by recent advances in ultra-low-power technology. Each sensor continuously measures parameters of interest and sends the data to a central device such as a personal digital assistant (PDA). Examples include sensors to observe brain activity for recording or warning against seizures, or sensors to examine health activity for diagnosis and automatic emergency calls.

Ultra-wideband (UWB) has recently received much attention as a promising air interface for short-range low data-rate communication scenarios matching the requirements of wireless biomedical applications [1], [2]. Furthermore, the Federal Communications Commission (FCC) has recently legalized a spectral mask between 3.1–10.6 GHz for UWB. Finally, the IEEE 802.15.4a Committee is developing a low-power UWB standard and has included body area networks (BANs) for medical and sport monitoring among their relevant application scenarios.[1]

Unfortunately, there are no detailed UWB BAN channel models required for wireless biomedical system design based on real measurements. Past attempts focus on finite-difference time-domain (FDTD) simulations for narrowband systems [3], [4] and UWB systems in the 3–6-GHz band [5]. The computational complexity of the FDTD method limited simulations to simple scenarios that do not include the impact of small UWB antennas placed near a body. Narrowband measurements near the body in the 2.4-GHz band [6], as well as UWB measurements in the 3–6-GHz band [7]–[11] have also been reported. However, these studies are mostly qualitative and do not provide a detailed analysis of the statistics or a model implementation recipe.

To address problems with body channel characterization, we have extracted statistics based on measurements of electromagnetic waves propagating around the torso. Using these statistics, we propose a model that is evaluated in terms of replicating the number of significant multipath components (MPCs), and the distribution of the rms delay spread. We focus on the 3–6-GHz band, which is an important portion of the FCC mask commonly proposed for UWB systems.

This paper discusses the results of our measurement campaign and proposes a computer implementation. Section II begins by presenting our measurement setup. This paper focuses on statistics measured due to diffraction around the torso (Section III) and reflection off of the ground (Section IV). Section V extends these results by considering the impact of arm motions. Section VI proposes a model and implementation recipe. Finally, Section VII summarizes our major conclusions.

II. Measurement Setup

The measurement setup used to extract the statistics of our model is summarized here. Reference [11] provides a more detailed description. We take measurements in the frequency range from 3 to 6 GHz. A vector network analyzer measures the $S21$-parameter between two antennas placed at various positions on a human body. All measurements are converted to the time domain using an inverse fast Fourier transform (IFFT) and a Hamming window to reduce sidelobes. The same small low-profile Skycross SMT-3TO10M[2] antennas are used for all measurements. These antennas are chosen since they accurately

Manuscript received August 1, 2005; revised August 12, 2006. This work was supported under the MEDEA+ Witness Project.

A. Fort is with the Interuniversity Microelectronics Centre (IMEC), B-3001 Leuven, Belgium, and also with the Fundamental Electricity and Instrumentation (ELEC) Department, Vrije Universiteit Brussel, B-1050 Brussel, Belgium (e-mail: forta@imec.be).

C. Desset is with the Interuniversity Microelectronics Centre (IMEC), B-3001 Leuven, Belgium.

P. De Doncker is with the Universite Libre Bruxelles (ULB)–Ondes et Signaux, B-1050 Bruxelles, Belgium.

P. Wambacq is with the Interuniversity Microelectronics Centre (IMEC), B-3001 Leuven, Belgium, and also with the Department of Department of Electronics and Informatics (ETRO), Vrije Universiteit Brussel, B-1050 Brussel, Belgium.

L. Van Biesen is with the Fundamental Electricity and Instrumentation (ELEC) Department, Vrije Universiteit Brussel, B-1050 Brussel, Belgium.

Digital Object Identifier 10.1109/TMTT.2006.872066

[1]IEEE 802.15.4a. [Online]. Available: http://www.ieee802.org/15/pub/TG4a.html

[2]Skycross, Melbourne, FL. [Online]. Available: http://www.skycross.com

TABLE I
PATH LOSS MODEL PARAMETERS

Parameter	*Parameter Value*
n	7.2
d_0	0.1 m
P_{0dB}	50.5 dB

represent the size and profile requirements typical of body worn sensor devices [2].

This paper focuses on propagation around the human torso. However, the procedure and results can be extended for other scenarios such as communication along the front of the body. The transmitter is placed at several positions along the front of the body, and the receiver is placed at various positions around the torso. A total of 144 measurements are taken to extract propagation statistics.

We found that the channel parameters change depending on the receiver position around the torso. To describe this phenomenon easily, we define three regions. The "front" corresponds to measurements taken from 0° to $\pm 60^\circ$, the "side" corresponds to measurements taken from $\pm 60^\circ$ to $\pm 160^\circ$, and the "back" corresponds to measurements taken from $\pm 160^\circ$ to $\pm 180^\circ$.

Finally, the separation of the antenna and body has a strong impact on the path loss [11]. We control this separation by placing a 5-mm dielectric between the body and antenna. The antenna is taped to the dielectric and held against the body using tight elastics.

III. DIFFRACTION AROUND THE TORSO

The path loss, power delay profile (PDP), and amplitude statistics of signals diffracting around the body is described here.

A. Path Loss

FDTD simulations [5] and measurements [12] have shown that paths traveling through the body in the gigahertz range are significantly attenuated. Instead, waves diffract around the torso. Therefore, we measure the distance around the perimeter of the body when modeling the path loss. Equation (1) and Table I summarizes the empirical power decay law extracted from our measurements. For a detailed description of this model, refer to [11]

$$P_{\mathrm{dB}} = P_{0dB} + 10n \log\left(\frac{d}{d_0}\right). \tag{1}$$

The parameter n is called the path loss exponent, d is the distance from the antenna, d_0 is the reference distance, and $P_{0\,\mathrm{dB}}$ is the path loss at the reference distance.

B. PDP

A convenient characterization of multipath propagation channels is the discrete-time impulse response model [13], [14]. In this model, the time axis is divided into small time intervals called "bins." The received power is integrated within each bin to obtain the energy received as a function of excess delay. The first bin corresponds to the first received MPC and its time of arrival is determined manually. Each bin is assigned an amplitude corresponding to the energy in that bin. The bin size is generally chosen to be the resolution of the measurement since two paths arriving within a bin cannot be resolved. The measurement resolution is approximated as the reciprocal of the bandwidth swept (0.33 ns) multiplied by the additional window function bandwidth. The 6-dB bandwidth of the Hamming window is 1.5 times wider than the rectangular window, resulting in a 0.5-ns resolution. We observed a "dense" impulse response where each bin contains significant energy above the noise.

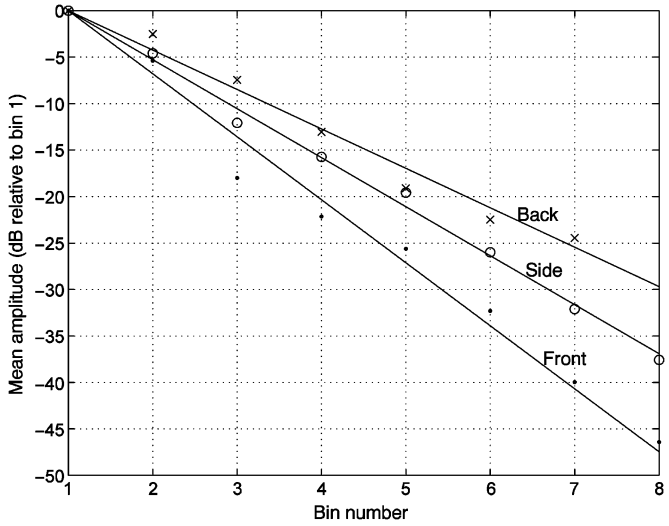

Fig. 1. Decrease in mean amplitude over successive 0.5-ns bins, relative to the first bin. The receiver is worn on the front, side, or back.

By averaging the energy in each bin over all the observations, we obtain the average PDP (see Fig. 1). The vertical axis shows the average bin energy relative to the average energy in the first bin. The horizontal axis indicates the bin number. Individual points correspond to the average energy in each bin, while the straight line is obtained by a best-fit procedure. Energy decay versus excess delay is commonly modeled with an exponential law [15]. Fig. 1 shows that this is also a reasonable approximation for body area systems, as illustrated by the linear fit on a decibel scale. The decay rates depend on the position of the body, and will be discussed in Section VI.

In general, there is a longer impulse response on the back and side of the body compared with the front of the body. Since only negligible signal energy is expected inside the body, this effect is probably due to echoes off of the body itself and because there are more ways in which a signal can arrive at the receiver when it is placed on the opposite side of the torso. For example, the signal can diffract around the body in both clockwise and counterclockwise directions, as well as around the shoulders and arms.

C. Amplitude Distribution

In addition to the large-scale path-loss trend around the human body, a reliable statistical model is needed to determine how much the signal level can vary. In UWB systems, each

resolved channel component is due to a small number of scatterers and the amplitude distribution in each bin can be different [14]. Therefore, we extract the amplitude distribution of every bin individually.

To determine the amplitude distribution, the large-scale path loss law (1) is removed. Several distributions are fit to the resulting data including the Lognormal, Nakagami-m, and Rayleigh distributions. We use the parameter estimators from [16] for the Nakagami-m distribution, while maximum likelihood (ML) estimates are used for the other distributions. Here, these distributions are compared against the measured data, while Section VI describes the actual parameter values. Contrary to previous channel studies, we use the Akaike information criterion (AIC) rather than a hypothesis test for selecting the best model among the set of candidates. Thus, before comparing distributions, we briefly review the Akaike criterion.

1) Akaike Criterion: The second-order AIC (AIC_c) is defined as follows [17]:

$$\mathrm{AIC}_c = -2\log_e\left(\ell(\hat{\theta}|\mathrm{data})\right) + 2K + \frac{2K(K+1)}{(n-K-1)} \qquad (2)$$

where $\log_e(\ell(\hat{\theta}|data))$ is the value of the maximized log-likelihood over the unknown parameters (θ), given the data and the model, K is the number of parameters estimated in that model, and n is the sample size. This equation is straightforward to compute since the log likelihood is readily available from the ML estimates. Intuitively, the first term indicates that better models have a *lower* AIC_c because the log-likelihood reflects the overall fit of the model to the data. The second part of the equation penalizes additional parameters ensuring we select models that best fits the data with the least number of parameters. The AIC_c also has a strong theoretical motivation since it provides an estimate of the Kullback–Leibler information loss [18]. In this way, the model with the lowest AIC_c approximates the "true" distribution with the minimum loss of information.

In practice, the value of the AIC_c by itself has no meaning. However, the relative values of AIC_c among the models can be used to rank the models from best to worst and to provide a strength of evidence that one model is better than another. To facilitate this, the two following related metrics are normally reported:

$$\Delta_i = \mathrm{AIC}_{c,i} - \min(\mathrm{AIC}_c) \qquad (3)$$

$$w_i = \frac{\exp\left(-\frac{\Delta_i}{2}\right)}{\sum_{r=1}^{R}\exp\left(-\frac{\Delta_r}{2}\right)} \qquad (4)$$

where AIC_i is the AIC value for model index i, and R is the number of models. Clearly, the best model among the set of models has a delta AIC of 0. As a rule-of-thumb, $\Delta_i < 2$ suggests substantial evidence for the model, values between 3–7 indicate that the model has considerably less support, while values greater than ten indicate that the model is very unlikely [17]. The Akaike weights (w_i) provide a more precise measure of the strength of evidence and can be interpreted as the probability that the model is the best among the whole set of candidates. In addition, the ratio of two AIC weights indicates how much more likely one model is better compared to the other. Clearly, these metrics are more informative than a simple hypothesis test that can only pass or fail a model based on an arbitrary significance level without providing any strength of evidence or ranking. These advantages will become more apparent as we apply the metrics to our data in the following sections. For more information about the Akaike criterion, refer to [17].

TABLE II
COMPARISON OF FADING MODELS OF THE FIRST BIN

Model	*Front*		*Side*		*Back*	
	Δ	w	Δ	w	Δ	w
$Lognormal$	0.0	1.0	0.0	0.96	0.0	0.71
$Nakagami-m$	26.2	0.0	6.5	0.04	8.7	0.01
$Rayleigh$	30.4	0.0	12.4	0.0	1.8	0.29

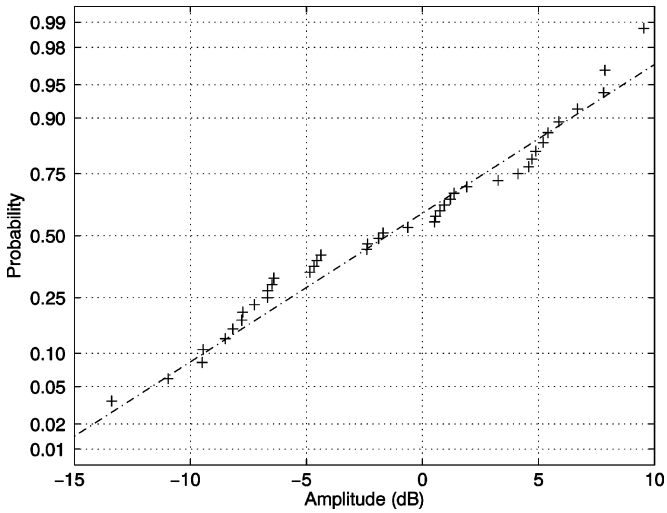

Fig. 2. Scatter plot of the energy from the first bin (side of the body) plotted against ideal values of the normal distribution. A straight line indicates the data is normal.

2) Comparison of Distributions: Table II shows the AIC deltas and weights obtained when fitting the Lognormal, Nakagami-m, and Rayleigh distributions to the distribution of the energy integrated over the first bin. Results are reported separately for measurements taken along the front, side, and back of the body.

Clearly, the delta AIC values show that the Lognormal model provides a superior fit to the data for all receiver positions. This is particularly true along the front and sides of the body where the AIC weights indicate the Nakagami-m and Rayleigh distributions have only negligible probability of being the best model in the set. While we only present results for the first bin, similar conclusions are obtained for most of the other bins.

One drawback of using the AIC criterion is it can only be used to test models relative to other models in the set. It is entirely possible that *none* of the models in the set provide a reasonable fit to the data, and this would not be apparent from Table II alone. We, therefore, confirm the Lognormal distribution graphically. Fig. 2 shows the normal probability plot taken from measured data extracted from the first bin along the side of the body. The

data appears linear on this scale confirming the Lognormal distribution provides a good fit to the data.

In addition to the empirical evidence supporting the Lognormal distribution, we can propose a physical explanation. It is likely that a large number of effects contribute to the attenuation of the signal including diffraction, reflection, energy absorption, antenna losses, etc. Most of these effects are multiplicative, or equivalently additive in the log domain. By the central limit theorem, a large number of random multiplicative effects will converge to a normal distribution in the log domain. Along the side and back of the body, there are also likely to be additive effects due to the combination of multiple paths around the body or reflections off of the arms, shoulders, etc. However, it can be shown that adding together Lognormal variables results in a distribution that can be well approximated by another Lognormal distribution [19].

The Rayleigh distribution is a significantly poorer model along the front of the body. This distribution is observed when several paths of equal amplitude and random phase combine at the receiver. However, along the front of the body, there are no unresolvable paths of significant amplitude other than the direct path so this distribution is not physically justified. However, the Rayleigh AIC weights gradually increase as the receiver is placed further away from the transmitter. For example, the last column of Table II indicates some uncertainty as to whether the Lognormal or Rayleigh distribution provides the best fit. A plausible explanation is that the signal arrives at the receiver on the back of the body via multiple paths due clockwise and counterclockwise diffraction around the body, diffraction over the shoulders, and reflections off the arms. If enough of these paths have a large amplitude and combine randomly at the receiver, the Rayleigh distribution can also plausibly fit the data.

Finally, under no circumstances does the Nakagami-m distribution provide any advantage over the other models. It is substantially worse than the Lognormal distribution for all antenna positions, and does not provide any advantage over the Rayleigh distribution on the back of the body.

3) Correlation Between Bins: Past channel studies have shown that there is often substantial correlation between the amplitudes of adjacent bins [5], [13], [20]. We calculate the correlation coefficient between the log amplitudes of each bin. In all cases, high correlation coefficients are observed between adjacent bins (ρ between 0.65–0.8) and gradually decreases for nonadjacent bins. High correlation can result from a number of expected physical effects including wavelength dispersion as the signal diffracts around the torso, overlapping path trajectories in the vicinity of the antenna, and a symmetry of the body.

IV. Ground Reflections

It is shown in [8], [11] that ground reflections can influence the total received energy when the receiver is placed on a different side of the body as the transmitter. We can clearly identify ground reflections arriving approximately 7–10 ns after the initial diffracting wave, as previously reported in [5], [8], [11]. In order to characterize reflections, we manually identify their location and bin the resulting data, as described in Section III-C.3. The Lognormal, Nakagami-m, and Rayleigh models are fit to the resulting distribution of the energy received in each bin. Finally, the Akaike criterion (Section III-C.1) is applied to test the validity of each model. Table III summarizes the results of this comparison for the first bin.

TABLE III
COMPARISON OF FADING MODELS OF THE FIRST BIN

	Front		*Side*		*Back*	
Model	Δ	w	Δ	w	Δ	w
$Lognormal$	0.0	1.0	0.0	0.55	0.0	0.60
$Nakagami-m$	23.7	0.0	0.9	0.35	1.0	0.21
$Rayleigh$	21.0	0.0	3.5	0.10	0.3	0.19

TABLE IV
ENERGY FLUCTUATION OF THE FIRST BIN DUE TO ARM MOTIONS

	Side		*Back*	
Model	Δ	w	Δ	w
$Lognormal$	4.4	0.1	0.0	0.77
$Nakagami-m$	0.0	0.9	2.4	0.23
$Rayleigh$	1139	0.0	573	0.0

In each case, the Lognormal distribution provides a superior fit to the data. It is particularly more effective along the front of the body where the AIC weights indicate only a negligible probability that one of the other models is the best in the set. As in Fig. 2, normal plots are used to graphically confirm that the Lognormal distribution provides a plausible model. The same physical interpretation of a large number of multiplicative effects given in Section III-C.3 may also apply to floor reflections.

A similar trend as in Table II is observed where the Rayleigh and Nakagami-m AIC weights are higher when the receiver is worn on the side or back. This may be due to secondary reflections off the arms, and legs arriving with approximately equal amplitude and random phase at the receiver.

As shown in Section III-C, the PDP decays approximately exponentially and there is substantial correlation between adjacent bins. Lognormal parameters, decay rates, and correlations extracted from measurements will be presented in Section VI.

V. Arm Motions

Plots of the impulse response versus arm position given in [11] clearly show reflections off the arms of the body can interfere with signal paths diffracting around the torso. To model the impact of arm motions, we measure the signal variation over time as a person walks in place. We do not consider the case when the receiver is on the front of the body since the arms are too far away to influence the received power [11]. Over 100 measurements are made at 12 different antenna positions along the side and back of the body. For a detailed description of this experiment setup, refer to [11].

Fluctuation around the mean energy for each bin is recorded and the Lognormal, Nakagami-m, and Rayleigh distributions are fit to the resulting data. As in Section III, we compare the relative accuracy of these models using the Akaike criterion. Table IV summarizes the results for the first bin.

The high delta AIC values obtained for the Rayleigh distribution indicate that it is a very poor fit to the data compared with the other models. This is likely due to a combination of two effects. First, the arms do not produce enough random phase signal paths by themselves to justify the Rayleigh distribution.

TABLE V
NAKAGAMI-m PARAMETERS FOR FADING DUE TO ARM MOTIONS

Bin number	*Side*	*Back*
1	9.6	3.0
2	3.6	2.2
3	1.8	1.7

Second, the resolution of our measurement is very high so that there are not many unresolvable MPCs.

The Lognormal and Nakagami-m distributions perform significantly better. The signal fluctuation is due to a small number of random phase paths adding at the receiver. Therefore, neither of these distributions has a strong physical motivation. However, there is substantial empirical evidence from other UWB measurement campaigns indicating that these distributions often provide a plausible fit to measurements in this situation [14], [21]. Plots comparing the CDF of the measured data with the Lognormal and Nakagami-m models confirm the excellent fit for our data as well.

We do not have enough data points to confidently determine which of these distributions is better. In most bins, the Nakagami-m AIC deltas are slightly lower. However, the Akaike weights indicate a high uncertainty. Since both distributions are very similar, we conclude that either the Lognormal or Nakagami-m distributions could be used to model energy fluctuations due to arm movements. Models such as the Rayleigh distribution having no parameters to control the degree of fading are grossly pessimistic and should not be used.

The m-parameters of the Nakagami-m distribution extracted from measurements in the first three bins are provided in Table V. Notice that m tends to be lower on the back of the body and decreases with increasing excess delay. This is consistent with other UWB measurements [14]. It is likely that movements result in more unresolvable paths on the back of the body so the Nakagami-m distribution begins to approach the Rayleigh distribution corresponding to $m = 1$. Furthermore, a decreasing m-parameter indicates that later arriving MPCs are more diffuse than earlier components which agrees with intuition [14].

VI. MODEL IMPLEMENTATION

Sections III and IV present a statistical analysis discussing the kinds of distributions and a physical interpretation. The extracted parameters and proposes an implementation for a body area channel model are detailed here.

We can obtain a discrete time model of the channel impulse response due to signals diffracting around the torso by recreating the energy distributions of each bin extracted from measurements in Section III. We have found that correlated Lognormal distributions provide the best fit to the data overall regardless of the position of the receiver. We, therefore, recommend modeling body area propagation using correlated Lognormal variables to represent the gain of each bin.

We can generate an N_b element vector of correlated lognormal variables using the same procedure outlined in [22]. N_b is the number of bins containing significant energy. Measurements indicate that $N_b = 8$ is sufficient on all sides of the body.

TABLE VI
MODEL PARAMETERS, DIFFRACTION AROUND THE TORSO

Parameter	*Front*	*Side*	*Back*
μ (dB relative to P_{dB})	-1.1	-1.8	-1.6
σ (dB)	5.4	6.7	4.6
λ (dB/bin)	-7.2	-5.7	-4.7
ρ	0.83	0.86	0.80

We first generate a vector X of N_b uncorrelated zero-mean unit-variance normal variables. X is then post multiplied by the upper triangular Cholesky factorization of the covariance matrix (C) to introduce the correlation and variances. Finally, the mean amplitude of each bin (M) and the appropriate distance related path loss (P_{dB}) are applied. This procedure can be summarized as follows:

$$G_{k,\mathrm{dB}} = Xchol(C) - M - P_{\mathrm{dB}}(d) \tag{5}$$

where $G_{k,\mathrm{dB}}$ represents the gain of bin k expressed in decibels, C is the N_b by N_b covariance matrix extracted from the measured correlation coefficients and variances, and M is the N_b element vector of means for each bin. Vector M is defined relative to the path loss $P_{\mathrm{dB}}(d)$ given by (1). The decibel gains from (5) are then converted to the linear domain.

While the model in (5) very accurately recreates the statistics of the measured impulse responses, it requires many parameters (vector M and covariance matrix C) to define the means, variances, and correlations of every bin individually.

We propose three simplifications to more compactly describe the channel. First, Fig. 1 shows that the mean energy in each bin decays approximately linear in the log domain. Thus, we can replace the vector M by two parameters, i.e., μ and λ, describing the mean energy in decibels of the first bin and the decay rate in decibels/bin, respectively. Second, the estimated variances of each bin do not change substantially as a function of excess delay. This motivates using a single variance to model all the bins. Finally, we observe high correlations in adjacent bins, but gradually lower correlations between nonadjacent bins. Therefore, a reasonable approximation is to enforce correlation between adjacent bins only. The last two simplifications allow us to replace the covariance matrix C by two parameters ρ and σ, representing correlation between the adjacent bins and the standard deviation of each bin.

Using these simplifications, the body area propagation channel can now be described with only four parameters given in Table VI extracted from measurements at different locations on the body. The following can be used to generate the N_b bins having the specified correlation coefficient in adjacent bins

$$g_k = \rho g_{k-1} + n_k\sqrt{1-\rho^2} \tag{6}$$

$$G_{k,\mathrm{dB}} = \sigma g_k - P_{\mathrm{dB}}(d) + \mu + \lambda(k-1). \tag{7}$$

Equation (6) uses zero mean, unit variance, uncorrelated normal variables n_k to generate g_k such that g_k and g_{k-1} have the specified correlation coefficient. The appropriate standard deviations and means are then added to generate $G_{k,\mathrm{dB}}$, the gain in decibels of bin k $(k > 0)$.

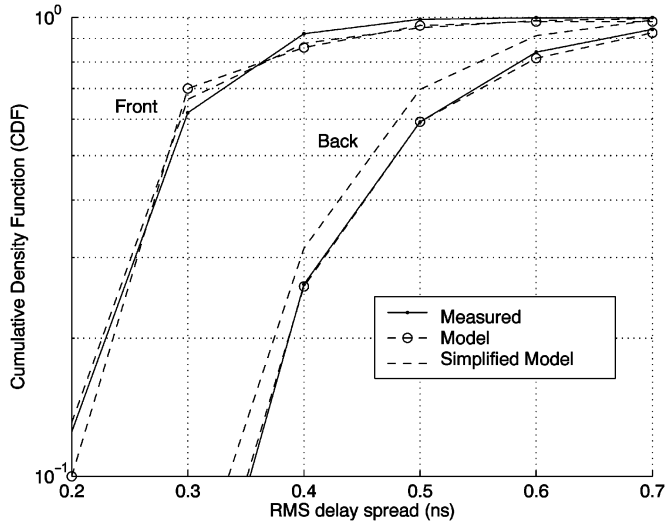

Fig. 3. Comparison of the measured and modeled rms delay spread distribution. Receiver worn on the front and back of the torso.

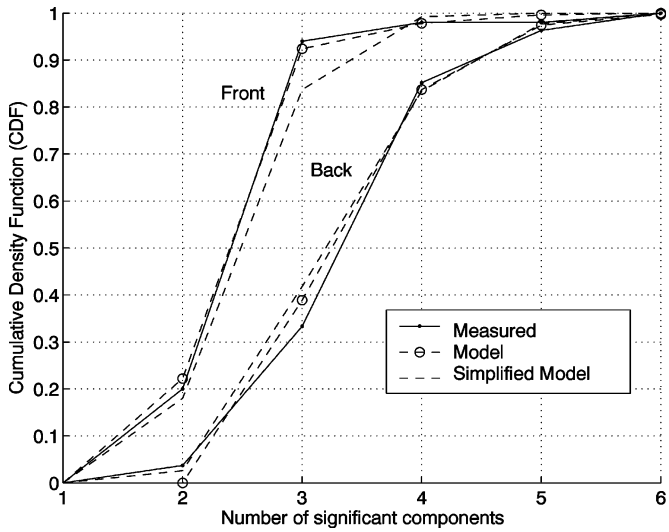

Fig. 4. Comparison of the measured and modeled distribution of the number of significant bins. Receiver worn on the front and back of the torso.

Two metrics frequently used to verify channel models are the rms-delay spread $(\tau_{\rm rms})$, and the number of bins within 10 dB of the largest bin $(N_{10\,\rm dB})$ [21]. By comparing these metrics between simulated and measured impulse responses, we ensure that channels generated with our model are spread over the same amount of time and have the same number of significant resolvable MPCs.

Figs. 3 and 4 compare the distributions of $\tau_{\rm rms}$ and $N_{10\,\rm dB}$ extracted from measurements, and generated with a computer using (5) or (7). For clarity, we only show distributions representing impulse responses when the receiver is worn on the front and back of the body. Clearly, both models accurately reproduce the basic characteristics of the measured impulse responses. As expected, the simplified model is slightly less accurate. However, the discrepancy is very small, justifying the greatly simplified representation.

TABLE VII
MODEL PARAMETERS, GROUND REFLECTION

Parameter	*Front*	*Side*	*Back*
μ (dB relative to P_{0dB})	-34.0	-39.7	-44.3
σ (dB)	4.6	3.9	3.9
λ (dB/bin)	-5.0	-5.6	-6.3
ρ	0.77	0.71	0.66

Ground reflections arrive between 7–10 ns later depending on the exact position of the receiver and the height of the body. As indicated in Section IV, these reflections are well modeled by Lognormal variables in a similar manner as the signal components diffracting around the torso. Therefore, the ground reflection bins can also be generated using either (5) or (7). Table VII provides parameters extracted from our measurements. Visual inspection of $\tau_{\rm rms}$ and $N_{10\rm dB}$ CDFs shows a similarly good match as in Figs. 3 and 4.

Finally, the influence of arm motions for receivers on the side or back of the body can be introduced by superimposing a fading distribution on the mean amplitudes for each bin. Section V indicates a Nakagami-m distribution with the parameters from Table V provides a good fit to our data.

VII. CONCLUSIONS

Using UWB sensors for health monitoring around the body is a promising new wireless application. Unfortunately, there are very few measurements or models describing the body area propagation channel. This paper analyzes statistics and proposes a model implementation based on an extensive measurement campaign. Using an information theoretical criterion, we have shown that the distribution of the received energy due to diffraction and floor reflections is well modeled by correlated log-normal variables. Furthermore, we show that the fluctuation in the received energy due to typical arm motions are better described by distributions having extra parameters to vary the amount of fading, such as the Lognormal and Nakagami-m distributions, compared with a Rayleigh model. Finally, we have presented a complete model implementation and suggested practical simplifications.

REFERENCES

[1] R. Shmidt *et al.*, "Body area network, a key infrastructure element for patient-centered medical applications," *Biomed. Tech. (Berl)*, vol. 47, pp. 365–368, 2002.

[2] B. Gyselinckx, C. Van Hoof, J. Ryckaert, R. F. Yazicioglu, P. Fiorini, and V. Leonov, "Human++: Autonomous wireless sensors for body area networks," in *Proc. IEEE Custom Integr. Circuits Conf.*, Sep. 2005, pp. 12–19.

[3] B. Latre, G. Vermeeren, I. Moerman, L. Martens, F. Louagie, S. Donnay, and P. Demeester, "Networking and propagation issues in body area networks," in *Proc. SCVT*, 2004.

[4] J. Ryckaert, P. DeDoncker, S. Donnay, A. Delehoye, and R. Meys, "Channel model for wireless communication around the human body," *Electron. Lett.*, vol. 40, no. 9, pp. 543–544, Apr. .

[5] A. Fort, C. Desset, J. Ryckaert, P. DeDoncker, L. VanBiesen, and S. Donnay, "Ultra wideband body area channel model," in *Proc. ICC* , Seoul, Korea, 2005, pp. 2840–2884.

[6] P. Hall, M. Ricci, and T. Hee, "Measurements of onbody propagation characteristics," in *Int. Microw. Millimeter Wave Technol. Conf.*, 2002, pp. 770–772.

[7] T. B. Welch, R. L. Musselman, B. A. Emessiene, P. D. Gift, D. K. Choudhury, D. N. Cassadine, and S. M. Yano, "The effects of the human body on UWB signal propagation in an indoor environment," *IEEE J. Select. Areas Commun.*, vol. 20, no. 9, pp. 1778–1782, Sep. 2002, . : .
[8] T. Zasowski, F. Althaus, M. Stager, A. Wittneben, and G. Tröster, "UWB for noninvasive wireless body area networks: Channel measurements and results," in *IEEE Ultra Wideband Syst. Technol. Conf.*, 2003, pp. 285–289.
[9] I. Z. Kovacs, G. F. Pedersen, P. C. F. Eggers, and K. Olesen, "Ultra wideband radio propagation in body area network scenarios," in *Proc. ISSSTA*, 2004, pp. 102–106.
[10] I. Z. Kovacs and P. Eggers, "Technical deliverable D4.2: UWB radio channel characterization for portable user terminal scenarios," Tech. Rep., Oct. 2004 [Online]. Available: http://cpk.auc.dk/FACE
[11] A. Fort, C. Desset, J. Ryckaert, P. DeDoncker, L. VanBiesen, and P. Wambacq, "Characterization of the ultra wideband body area propagation channel," in *Proc. ICU*, Zurich, Switzerland, 2006, pp. 22–27.
[12] T. Zasowski, G. Meyer, F. Althaus, and A. Wittneben, "Propagation effects in UWB body area networks," in *Proc. ICU*, 2005, pp. 16–21.
[13] H. Hashemi, "Impulse response modeling of indoor radio propagation channels," *IEEE J. Select. Areas Commun.*, vol. JSAC-5, no. 7, pp. 967–977, Sep. 1987.
[14] D. Cassioli, M. Z. Win, and A. F. Molisch, "The elutriate bandwidth indoor channel: From statistical model to simulations," *IEEE J. Select. Areas Commun.*, vol. 20, no. 6, pp. 1247–1257, Jun. 2002.
[15] A. Saleh and R. A. Valenzuela, "A statistical model for indoor multipath propagation," *IEEE J. Select. Areas Commun.*, vol. JSAC-5, no. 2, pp. 128–137, Feb. 1987.
[16] Q. T. Zhang, "A note on the estimation of the Nakagami-m fading parameter," *IEEE Commun. Lett.*, vol. 6, no. 6, pp. 237–238, Jun. 2002.
[17] K. P. Burnham and D. R. Anderson, *Model Selection and Multimodel Inference: A Practical Information-Theoretic Approach*, 2nd ed. New York: Springer-Verlag, 2002.
[18] H. Akaike, "Information theory as an extension of the maximum likelihood principle," in *Proc. 2nd Int. Inf. Theory Symp.*, 1973, pp. 267–281.
[19] L. Fenton, "The sum of log-normal probability distributions in scatter transmission systems," *IEEE Trans. Commun. Syst.*, vol. CS-8, no. 1, pp. 57–67, Jun. 1960.
[20] G. L. Turin, F. D. Clapp, T. L. Johnston, S. B. Fine, and D. Lavry, "A statistical model of urban multipath propagation," *IEEE Trans. Veh. Technol.*, vol. VT-21, no. 1, pp. 1–9, Feb. 1972.
[21] A. F. Molisch *et al.*, "A comprehensive model for ultrawideband propagation channels," in *Globecom*, 2005, pp. 3648–3653.
[22] P. Z. Peebles, Jr., *Probabiltiy, Random Variables, and Random Signal Principles*. Englewood Cliffs, NJ: McGraw-Hill, 1993.

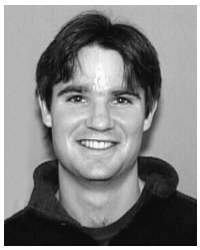

Andrew Fort (S'04) was born in Ottawa, ON, Canada, in 1975. He received the Bachelor degree in computer engineering from the University of Victoria, Victoria, BC, Canada, in 1998, and is currently working toward the Ph.D. degree at Vrije Universiteit Brussel, Brussels, Belgium.

As part of his cooperative study program, he was with Sanyo Electric, Gifu, Japan, where he developed hardware for digital cellular phones. Upon graduation, he was with IVL Technologies, Victoria, BC, Canada, where he designed digital signal processing (DSP) algorithms for pitch recognition of the human voice. In January 2000, he joined the Interuniversity Microelectronics Centre (IMEC), Leuven, Belgium, where he was involved in the research and development of a wide range of communication systems including satellites, multiple antennas, and wireless local area networks. He is currently with the Vrije Universiteit Brussel, where he is involved with ultra-low-power medical sensors and body area communication networks.

Claude Desset (S'94–M'01) was born in Bastogne, Belgium, in 1974. He received the Masters degree (*summa cum laude*) in electrical engineering and Ph.D. degree from the Université Catholique de Louvain (UCL), Louvain-la-Neuve, Belgium, in 1997 and 2001, respectively.

In 2001, he joined the Interuniversity Microelectronics Centre (IMEC), Leuven, Belgium, where he is currently a Senior Researcher involved in the design of wireless communication systems. He currently focuses on ultra-low-power personal area networks, but also has interests in multiinput–multioutput (MIMO), link adaptation, and turbo coding.

Philippe De Doncker received the Masters degree in physics engineering and Ph.D. degree from the Université Libre de Bruxelles, Belgium, in 1996 and 2001, respectively.

He is currently an Assistant Professor with the Université Libre de Bruxelles. His research is focused on propagation and statistical methods for wireless communications.

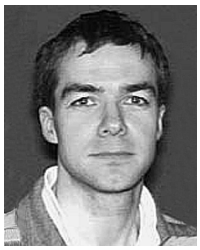

Piet Wambacq (S'89–M'91) received the M.Sc. degree in electrical and mechanical engineering and Ph.D. degree from the Katholieke Universiteit Leuven, Louvain-la-Neuve, Belgium, in 1986 and 1996, respectively.

Since 1996, he has been a Principal Scientist with the Interuniversity Microelectronics Centre (IMEC), Leuven, Belgium. He is also a Lecturer with the Vrije Universiteit Brussel, Brussels, Belgium. He has authored or coauthored two books and over 100 papers, international journals, and conference proceedings. He holds two patents. His research interests are design and computer-aided design (CAD) of mixed-signal and RF integrated circuits.

Dr. Wambacq has been an associate editor of the IEEE TRANSACTIONS ON CIRCUITS AND SYSTEMS—PART I: FUNDAMENTAL THEORY AND APPLICATIONS from 2002 to 2004. He is a member of the Program Committees of international conferences (e.g., DATE). He was the corecipient of the Best Paper Award at the Design, Automation, and Test (DATE) Conference in 2002 and 2005.

Leo Van Biesen (M'90) was born in Elsene, Belgium, on August 31, 1955. He received the Electro-Mechanical Engineer and Doctoral (Ph.D.) degrees from Vrije Universiteit Brussel (VUB), Brussels, Belgium, in 1978 and 1983, respectively.

He is currently he is a Full Senior Professor with VUB, where he teaches courses on fundamental electricity, electrical measurement techniques, signal theory, computer-controlled measurement systems, telecommunication, underwater acoustics, and geographical information systems for sustainable development of environments. His current interests are signal theory, modern spectral estimators, time-domain reflectometry, xDSL, and wireless local area networks (WLANs), fourth-generation (4G) mobile communication, underwater acoustics, and expert systems for intelligent instrumentation.

Prof. Van Biesen was elected and installed as president of IMEKO during the XVII World Congress, Dubrovnik, Croatia, in June 2003.